*Structural Engineering and Mechanics, Vol. 11, No. 1 (2001) 105-122*
DOI: http://dx.doi.org/10.12989/sem.2001.11.1.105


# Mixed formulated 13-node hexahedral elements with rotational degrees of freedom: MR-H13 elements

Chang-Koon Choi†, Keun-Young Chung‡ and Eun-Jin Lee‡†

*Department of Civil Engineering, Korea Adavanced Institute of Science and Technology, Taejon 305-701, Korea*

**Abstract.** A new three-dimensional 13-node hexahedral element with rotational degrees of freedom, which is designated as MR-H13 element, is presented. The proposed element is established by adding five nodes to one of the six faces of basic 8-node hexahedral element. The new element can be effectively used in the connection between the refined mesh and the coarser mesh. The derivation of the current element in this paper is based on the variational principles in which the rotation and skew-symmetric stress are introduced as independent variables. Numerical examples show that the performance of the new element is satisfactory.

**Key words:** 13-node hexahedral element; rotation; variable-node element; finite element method.

## 1. Introduction

In many engineering practices, stress concentration phenomena occur in the regions where the abrupt geometrical changes exist and/or the concentrated load is applied. A relatively finer mesh is used in the area of higher stress gradient but a rather coarser mesh is used where the stress distribution is relatively uniform. The *h*-refinement is the most commonly used adaptive strategy that reduces the element sizes to create a finer mesh where the initial finite element mesh is not adequate for the prescribed error tolerance.

In the adaptive *h*-refinement procedure by using 8-noded regular hexahedral elements, the hanging nodes which are not connected directly to the nodes of neighboring element are inevitably generated as a result of local mesh refinement. One of the practical ways commonly used to cope with the problem is to impose the displacement constraints on the hanging nodes to enforce the inter-element compatibility between the refined and unrefined element (Gargo *et al*. 1983, Delvoo 1991, Chang and Choi 1992). However, since imposing too many constraint equations may lock the system (Cook 1981), the use of variable-node elements in the transition region to avoid such problems has attracted many investigators attention (Gupta 1978, Choi and Park 1989, Choi and Lee 1993, 1995).

The development of isoparametric hexahedral element by Iron (1971) may be one of the most significant contributions to the advancement of finite element technology. The earlier hexahedral element which has variable number of nodes from 8 to 20 did not have a node at the centroids of

† Institute Chair Professor
‡ Research Assistant Professor
‡† Graduate Student

face generating a hanging node in the subdivided region. Also the basic eight-node hexahedral element needs to be further improved for practical use since the element deforms in a shear mode even under the pure bending load. Choi and Lee (1993) established a series of non-conforming variable-node hexhaheral element with 8- to 27-nodes for adaptive mesh gradation to solve this problem. NC-V1 and NC-V2 are the variable-node non-conforming hexahedral elements developed by Choi and Lee (1993).

The behavior of the brick type 13-node elements with three translational degrees of freedom per node is similar to that of the original isoparametric element, i.e., the element deforms basically in a shear mode (elements C-V1 and C-V2 in Choi and Lee 1993). One of the ways to improve the behavior of a 13-node hexahedral element is to add the rotational degrees of freedom to the element making the element have six degrees of freedom per node. The rotational degrees of freedom are treated as independent variables in the variational principles (Reissner 1965, Hughes and Brezzi 1989). The skew-symmetric components of stress are introduced as the Lagrange multipliers to enforce the equality of independent rotations with the skew-symmetric components of displacement gradient. These rotational degrees of freedom are viewed as being particularly advantageous when the element is connected to other types of elements that have six degrees of freedom per node (Allman 1984, Ibrahimbegovic and Wilson 1991, Yunus, Pawlak and Cook 1991, Choi, Chung and Lee 1996).

In this paper, a new 13-node element with rotational degrees of freedom that is demanded most frequently in practice is considered at this initial stage of development of a series of hexahedral variable node elements. This type of elements can be effectively used in the adaptive mesh refinement by providing the transition zone where a locally refined mesh is connected to the existing coarse mesh through a minimum mesh modification. Several numerical tests were carried out to evaluate the validity and performance of the three dimensional 13-node hexahedral elements with rotational degrees of freedom.

## 2. Variational formulation and independent rotations

### *2.1. Mixed type formulation including independent rotations*

Reissner (1965) was the first to propose the 'mixed' variational principle with independent rotational fields. His work has been followed by many researchers' works, such as Hughes and Brezzi (1989) and Ibrahimbegovic, *et al*. (1991) . However, the Reissner's variational formulation is inappropriate for numerical applications and inconvenient for the interpolation of fields. For this reason, Hughes and Brezzi (1989) modified the Reissner's variational formulation to preserve the stability of the discrete problem.

A mixed type variational functional considering the effects of surface traction $\boldsymbol{t}$ and body force $\boldsymbol{f}$ in an element domain $\Omega^e$ can be given as

$$\Pi_\gamma^e(\boldsymbol{u},\boldsymbol{\psi},skew\boldsymbol{\sigma})=\frac{1}{2}\int_{\Omega^e}(symm\nabla\boldsymbol{u})\cdot C\cdot(symm\nabla\boldsymbol{u})d\Omega+\int_{\Omega^e}skew\boldsymbol{\sigma}^T\cdot(skew\nabla\boldsymbol{u}-\boldsymbol{\psi})d\Omega$$
$$-\frac{1}{2}\gamma^{-1}\int_{\Omega^e}|skew\boldsymbol{\sigma}|^2d\Omega-\int_{\Omega^e}\boldsymbol{u}\cdot\boldsymbol{f}d\Omega-\int_{\Gamma_\sigma^e}\boldsymbol{u}\cdot\bar{\boldsymbol{t}}d\Gamma-\int_{\Gamma_u^e}\boldsymbol{t}\cdot\bar{\boldsymbol{u}}d\Gamma \quad (1)$$

where $\boldsymbol{u}$, $\boldsymbol{C}$, $skew\boldsymbol{\sigma}$, and $\boldsymbol{\psi}$ are the displacement field, constitutive modulus, skew-symmetric stress

tensor, and rotation tensor in an element domain, respectively. $\bar{\boldsymbol{t}}$ and $\bar{\boldsymbol{u}}$ are respectively the prescribed surface traction and displacement on the element boundary. For the isotropic elasticity and a Dirichlet boundary value problem, it was suggested that $\gamma$ in Eq. (1) takes the same value as the shear modulus; i.e., $\gamma=\mu$ (Hughes and Brezzi 1989). With the Euler-Lagrange equation resulted from variations on Eq. (1), the rotation tensor $\boldsymbol{\psi}$ is related to skew-symmetric displacement gradient $skew\nabla\boldsymbol{u}$.

### 2.2. Independent fields and hierarchical displacement

The basic displacement field in the variational formulation can be interpolated using shape functions at any arbitrary point in an element and can be represented by vector form.

$$symm\nabla\boldsymbol{u}^h=\langle\frac{\partial u_1^h}{\partial x_1}\ \frac{\partial u_2^h}{\partial x_2}\ \frac{\partial u_3^h}{\partial x_3}\ \frac{\partial u_1^h}{\partial x_2}+\frac{\partial u_2^h}{\partial x_1}\ \frac{\partial u_2^h}{\partial x_3}+\frac{\partial u_3^h}{\partial x_2}\ \frac{\partial u_1^h}{\partial x_3}+\frac{\partial u_3^h}{\partial x_1}\rangle^T \tag{2}$$

$$\psi^h=\langle\psi_1^h\ \ \psi_2^h\ \ \psi_3^h\rangle^T \tag{3}$$

$$skew\nabla\boldsymbol{u}^h=\frac{1}{2}\langle\frac{\partial u_3^h}{\partial x_2}-\frac{\partial u_2^h}{\partial x_3}\ \frac{\partial u_1^h}{\partial x_3}-\frac{\partial u_3^h}{\partial x_1}\ \frac{\partial u_2^h}{\partial x_1}+\frac{\partial u_1^h}{\partial x_2}\rangle^T \tag{4}$$

The various configurations of the variable-node hexahedral element can be defined by *n*-node mapping selectively (Fig. 1)

$$\boldsymbol{x}^h=\sum_{i=1}^{n}N_i^e(\xi,\eta,\zeta)\boldsymbol{x}_i^e \tag{5}$$

where, $n$ is the number of physical nodes in an element, $\boldsymbol{x}^h$ represents global coordinates and $N_i^e$ is the conventional isoparametric shape function for each node of a variable-node element. A brief description of the shape functions used to define the variable-node hexahedral element was presented by Choi and Lee (1993). Among many possible configurations defined by Eq. (5), the

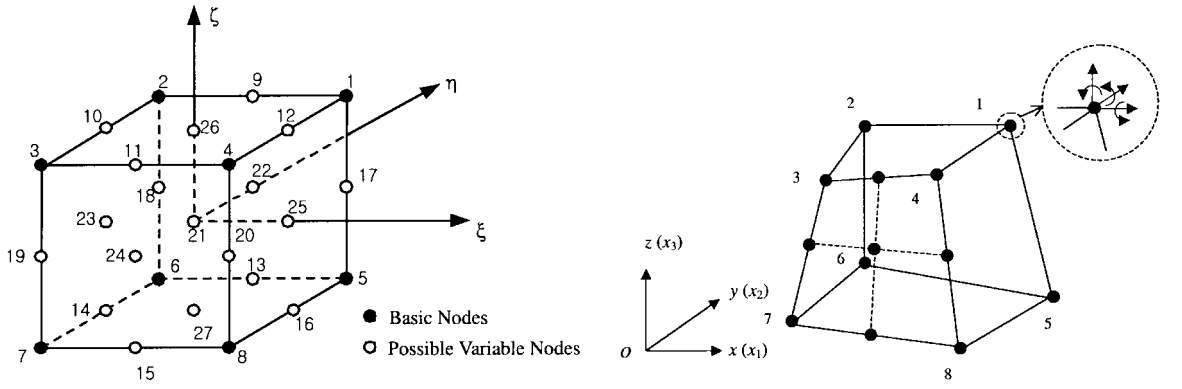


(a) Variable node elements in natural coordinate system (b) Degrees of freedom per node in a 13-node transition element

Fig. 1 Transition element with variable nodes

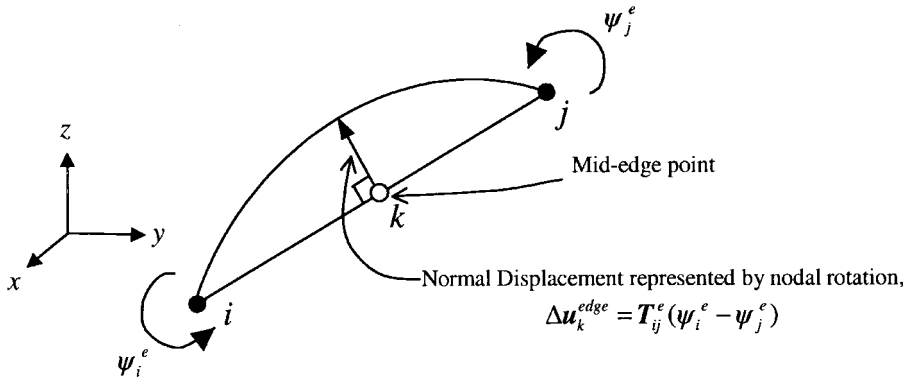


Fig. 2 One dimensional form of a hierachical edge displacement

hexahedral element with 13 nodes, which has additional 5 nodes on one of its faces, has been focused in this study (Fig. 1b).

The displacement interpolation for a 13-node element is derived by combining the conventional displacements of the parent element and the parabolic deformations of each edge which is the hierarchical displacement due to the addition of roational degrees of freedom.

$$\begin{pmatrix} u_1^h \\ u_2^h \\ u_3^h \end{pmatrix} = \boldsymbol{u}^h = \sum_{i=1}^{n} N_i^e(\xi,\eta,\zeta)\boldsymbol{u}_i^e + \sum_{k=n+1}^{n+m} N_k^{edge}(\xi,\eta,\zeta)\Delta\boldsymbol{u}_k^{edge} \quad (n=13,\ m=20) \tag{6}$$

where $\Delta\boldsymbol{u}_k^{edge}$ is the amplitude of hierarchical displacement at mid-edge point $k$ (Fig. 2), and $N_k^{edge}$ is the shape function which has a parabolic shape along the line joining adjacent two physical nodes, and $m$ is the number of mid-edge points which are used to define the hierarchical shape functions (Fig. 2). The hierarchical displacement component perpendicular to the element edge, which is used to improve the flexural behavior of element, can be replaced by the introduction of nodal rotations $\psi_i^e$. This transformation is analogous to the transformation of the one-dimensional flexural beam deformation due to the end rotations. The transformation of the mid-edge point displacements into the nodal rotations for an entire element is constructed by systematically using the same kind of transformation over each element edge. For the typical edge point $k$ defined by nodes $i$ and $j$ as shown in Fig. 2, the amplitude of mid-edge point deformation can be written as

$$\Delta\boldsymbol{u}_k^{edge} = \boldsymbol{T}_{ij}^e(\psi_i^e - \psi_j^e) \tag{7}$$

where,

$$\boldsymbol{T}_{ij}^e = \frac{1}{8}\begin{bmatrix} 0 & \Delta x_{3ij}^e & -\Delta x_{2ij}^e \\ -\Delta x_{3ij}^e & 0 & \Delta x_{1ij}^e \\ \Delta x_{2ij}^e & -\Delta x_{1ij}^e & 0 \end{bmatrix} \tag{7a}$$

$$\Delta\boldsymbol{x}_{ij}^e = \boldsymbol{x}_j^e - \boldsymbol{x}_i^e \tag{7b}$$

Thus, the one-dimensional transformation in the Eq. (7) can be directly applied to the displacement

interpolation in the global coordinate system to yield the following non-conventional displacement interpolation.

$$\boldsymbol{u}^h = \sum_{i=1}^{n} N_i^e(\xi,\eta,\zeta)\boldsymbol{u}_i^e + \sum_{k=n+1}^{n+m} N_k^{edge}(\xi,\eta,\zeta)\boldsymbol{T}_{ij}^e(\psi_i^e - \psi_j^e) \quad (n=13,\ m=20) \tag{8}$$

And the displacement field for the 13-node hexahedral element with rotational degrees of freedom can be rearranged as

$$\boldsymbol{u}^h = \sum_{i=1}^{n} \left[ N_i^e \boldsymbol{I} \quad \sum_k N_k^{edge} \boldsymbol{T}_{ij}^e \right] \begin{Bmatrix} \boldsymbol{u}_i^e \\ \psi_i^e \end{Bmatrix} \quad (n=13) \tag{9}$$

Unlike the translational displacement field, the independent rotational displacement field is interpolated in an isoparametric fashion over each element as

$$\psi^h = \begin{pmatrix} \psi_1^h \\ \psi_2^h \\ \psi_3^h \end{pmatrix} = \sum_{i=1}^{n} N_i^e(\xi,\eta,\zeta)\,\psi_i^e \quad (n=13) \tag{10}$$

The distribution of skew-symmetric stress for the mixed-type functional is assumed to be independent for each element and can be assumed as linear or parabolic polynomials given in the global coordinate system at the element level.

$$skew\ \sigma^h = \boldsymbol{S}^e \beta^e \tag{11}$$

where $\boldsymbol{S}^e$ is the skew-sysmetric stress distribution function and $\beta^e$ is a vector of skew-symmetric parameter which correspond to coefficients of assumed polynomials. The number of skew-symmetric stress parameters is an important factor for the element stabilization. When a small number of parameters is used, the spurious zero energy mode may occur. Thus, to suppress such undesired spurious zero energy modes, a requisite number of skew-symmetric interpolation parameters is necessary for a 13-node hexahedral element. The numerical test shows that in most cases 6 parameters are sufficient for 8-node hexahedral element (Ibrahimbegovic and Wilson 1991) and 9 parameters when the number of nodes per element is increased to thirteen (e.g., MR-H13 element, Choi and Chung 1995). The following matrix expressions are adopted for a skew symmetric stress distribution in this paper.

$$\boldsymbol{S}^e = \begin{bmatrix} 1 & x_1^h & 0 & 0 & 0 & 0 \\ 0 & 0 & 1 & x_2^h & 0 & 0 \\ 0 & 0 & 0 & 0 & 1 & x_3^h \end{bmatrix} \quad (\text{if } n=8) \tag{12}$$

$$\boldsymbol{S}^e = \begin{bmatrix} 1 & x_1^h & x_1^{h^2} & 0 & 0 & 0 & 0 & 0 & 0 \\ 0 & 0 & 0 & 1 & x_2^h & x_2^{h^2} & 0 & 0 & 0 \\ 0 & 0 & 0 & 0 & 0 & 0 & 1 & x_3^h & x_3^{h^3} \end{bmatrix} \quad (\text{if } n>8) \tag{13}$$

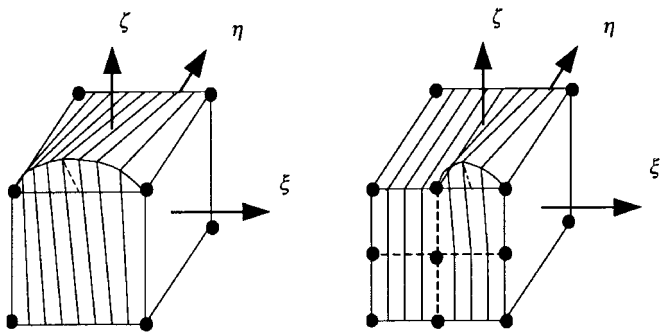


Fig. 3 Basic concept of hierarchical shape fuctions for 8-node & 13-node elements

### *2.3. Hierarchical shape function for 13-node hexahedral element*

The non-conventional displacement fields with rotational degrees of freedom in Eq. (9) can be obtained by the summation of conventional displacement field and edge-normal displacement due to nodal rotations. The conventional displacement fields are interpolated with the shape functions established by Choi and Lee (1993). The edge-normal displacement fields due to nodal rotations are interpolated with the transformation of hierarchical shape functions.

The hierarchical shape functions due to nodal rotations are of parabolic shape along each element edge. The hierarchical shape functions can be formed by multiplication of two basic functions. The first basic shape function has a parabolic shape along an edge (i.e., $\xi$ direction), and the second one is a combination of two linear functions in two perpendicular directions (i.e., $\eta$ and $\zeta$ directions) as shown in Fig. 3. The hierarchical shape functions for a 13-node hexahedral element should be further modified by considering the existence of nodes at each mid-edge.

The special hierarchical shape functions for the edges adjacent to corner node 4 in negative $\xi$-direction (Fig. 1a), i.e., for the edge joining node 4 and 3(or 11), can be constructed as follows:

$$N_{4,-\xi}^{edge}(\xi,\eta,\zeta)=H_1(\xi)H_2(\eta,\zeta) \tag{14}$$

where

$$H_1(\xi)=\begin{cases}2(|\xi|+\xi)(1-\xi) & \text{(if node 11 exists)}\\ 1-\xi^2 & \text{(otherwise)}\end{cases} \tag{14a}$$

$$H_2(\eta,\zeta)=\frac{1}{4}(1-\eta)(1-\zeta) \tag{14b}$$

The function of Eq. (14b) needs to be modified by the existence of variable nodes:

$$H_2(\eta,\zeta)=H_2(\eta,\zeta)-\frac{1}{2}\left\{\frac{1}{2}(1-|\eta|)(1+\zeta)\right\} \quad \text{(if node 26, or 10 \& 12 exist)} \tag{14c}$$

$$H_2(\eta,\zeta)=H_2(\eta,\zeta)-\frac{1}{2}\left\{\frac{1}{2}(1-\eta)(1-|\zeta|)\right\} \quad \text{(if node 24, or 19 \& 20 exist)} \tag{14d}$$

$$H_2(\eta,\zeta)=H_2(\eta,\zeta)+\frac{1}{4}\{(1-|\eta|)(1-|\zeta|)\} \quad \text{(if node 21, or 23 \& 25 exist)} \tag{14e}$$

If variable nodes 11 and 9 exist, the positive $\eta$ directional hierarchical shape functions from node 11 can be defined as

$$N_{11,+\eta}^{edge}(\xi,\eta,\zeta)=H_1(\eta)H_2(\xi,\zeta) \tag{15}$$

where

$$H_1(\eta)=\begin{cases}2(|\eta|-\eta)(1+\eta) & \text{(if node 26 exists)}\\ 1-\eta^2 & \text{(otherwise)}\end{cases} \tag{15a}$$

$$H_2(\xi,\zeta)=\frac{1}{2}(1-|\xi|)(1+\zeta) \tag{15b}$$

The Eq. (15b) needs to be modified by the addition of another variable node. In the case that the node 21 exists or both nodes 22 and 24 exist, the following modification is necessary.

$$H_2(\xi,\zeta)=H_2(\xi,\zeta)-\frac{1}{2}\{(1-|\xi|)(1-|\zeta|)\} \tag{15c}$$

In a similar manner, hierarchical shape functions of other edges can be established.

## 3. Element formulation

### *3.1. Element matrices*

The infinitesimal strains $symm\nabla \boldsymbol{u}^h$ in the variational functional (Eq. 1) can be defined as

$$symm\nabla \boldsymbol{u}^h=\sum_{i=1}^{n}(\boldsymbol{B}_i^e\boldsymbol{u}_i^e+\boldsymbol{G}_i^e\psi_i^e) \tag{16}$$

where $\boldsymbol{u}_i^e$ and $\psi_j^e$ are the nodal displacements and nodal rotations, respectively. The strain-displacement and strain-rotation matrices at a node $i$ are given as;

$$\boldsymbol{B}_i^{e^T}=\begin{bmatrix} N_{i,x}^e & & N_{i,y}^e & N_{i,z}^e \\ & N_{i,y}^e & N_{i,x}^e & N_{i,z}^e \\ & & N_{i,z}^e & N_{i,y}^e \; N_{i,x}^e \end{bmatrix} \quad (i=1, 2, ..., n) \tag{16a}$$

$$\boldsymbol{G}_i^e=\sum_{k}^{edges}\boldsymbol{B}_k^{edge}\boldsymbol{T}_{ij}^e \tag{16b}$$

Then, the discrete operator $\boldsymbol{G}_i^e$ needs to be modified to be capable of representing constant strain state. The modification fits into the framework of well-known B-bar methods (Ibrahimbegovic and Wilson 1991).

$$\overline{\boldsymbol{G}}^e=\boldsymbol{G}^e-\frac{1}{\Omega^e}\int_{\Omega^e}\boldsymbol{G}^e d\Omega \tag{17}$$

Furthermore, the infinitesimal rotation can be denoted as

$$skew\nabla \boldsymbol{u}^h - \psi^h = \sum_{i=1}^{n} (\boldsymbol{A}_i^e \boldsymbol{u}_i^e + \hat{\boldsymbol{F}}_i^e \psi_i^e) \tag{18}$$

where

$$\boldsymbol{A}_i^e = \frac{1}{2}\begin{bmatrix} 0 & -N_{i,z}^e & N_{i,y}^e \\ N_{i,z}^e & 0 & -N_{i,x}^e \\ -N_{i,y}^e & N_{i,x}^e & 0 \end{bmatrix} \quad (i=1, 2, ..., n) \tag{18a}$$

$$\hat{\boldsymbol{F}}_i^e = \boldsymbol{F}_i^e - N_i^e \boldsymbol{I} \tag{18b}$$

$\boldsymbol{I}$ is an unit matrix, and $\boldsymbol{F}_i^e$ can be obtained by the systematic transformation performed over the edges which meet at node $i$.

$$\boldsymbol{F}_i^e = \sum_{k}^{edges} \boldsymbol{A}_k^{edge} \boldsymbol{T}_{ij}^e \tag{19}$$

Minimizing the mixed variational functional $\Pi_\gamma$ in Eq. (1) for a single element, the following equations can be written

$$\begin{bmatrix} \boldsymbol{K}^e & \boldsymbol{H}^e \\ \boldsymbol{H}^{e^T} & -\boldsymbol{V}^e \end{bmatrix} \begin{Bmatrix} \boldsymbol{a}^e \\ \boldsymbol{\beta}^e \end{Bmatrix} = \begin{Bmatrix} \boldsymbol{f}_{ext}^e \\ \boldsymbol{0} \end{Bmatrix}; \qquad \boldsymbol{a}^e = \begin{Bmatrix} \boldsymbol{u}^e \\ \psi^e \end{Bmatrix} \tag{20}$$

where

$$\boldsymbol{K}^e = \int_{\Omega^e} [\boldsymbol{B}^e \;\; \boldsymbol{G}^e]^T \boldsymbol{C} [\boldsymbol{B}^e \;\; \boldsymbol{G}^e] d\Omega \tag{20a}$$

$$\boldsymbol{H}^{e^T} = \int_{\Omega^e} \boldsymbol{S}^{e^T} [\boldsymbol{A}^e \;\; \hat{\boldsymbol{F}}^e] d\Omega \tag{20b}$$

$$\boldsymbol{V}^e = \gamma^{-1} \int_{\Omega^e} \boldsymbol{S}^{e^T} \boldsymbol{S}^e d\Omega \tag{20c}$$

Since the skew-symmetric part of stress is interpolated independently in each element, the corresponding part of stiffness in Eq. (20) may be eliminated by the static condensation at the element level. Thus the remaining global degrees of freedom in an element are the nodal displacements $\boldsymbol{u}$ and nodal rotations $\psi$ as shown in Eq. (21).

$$(\boldsymbol{K}^e + \boldsymbol{H}^e \boldsymbol{V}^{e^{-1}} \boldsymbol{H}^{e^T}) \boldsymbol{a}^e = \boldsymbol{f}_{ext}^e \tag{21}$$

The element matrices $\boldsymbol{K}^e$, $\boldsymbol{H}^e$ and $\boldsymbol{V}^e$ in Eqs. (20a) through (20c) are basically computed by the 14-point quadrature. In the case that the number of nodes is greater than eight such as the case of 13-node element Gupta's subdomain integration concept (Gupta 1978, Fig. 4) needs to be used to integrate the discontinuous functions of element matirices. Thus, each subdomain is integrated by the 14-point quadrature first, and then the contributions of each subdomain are summed up to achieve the entire domain integration combined together.

The equivalent nodal forces due to surface traction and body forces are expressed as

$$\boldsymbol{f}_{ext}^e = \int_{\Omega^e} \boldsymbol{N}^{e^T} \boldsymbol{f}^h d\Omega + \int_{\Gamma_\sigma^e} \boldsymbol{N}^{e^T} \bar{\boldsymbol{t}}^h d\Gamma \tag{22}$$

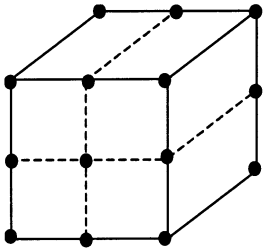

Fig. 4 Partitioning of integration domains of MR-H13

where shape function matrix $\boldsymbol{N}^e$ is

$$\boldsymbol{N}^{e^T} = \begin{bmatrix} \boldsymbol{N}_1^{e^T} \\ \boldsymbol{N}_2^{e^T} \\ \vdots \\ \boldsymbol{N}_n^{e^T} \end{bmatrix}, \quad \boldsymbol{N}_i^e = \begin{bmatrix} N_i^e \boldsymbol{I} & \sum_k^{edges} N_k^{edge} \boldsymbol{T}_{ij}^e \end{bmatrix} \tag{23}$$

In calculating the equivalent nodal force components related with rotational degrees of freedom, the traction $\bar{\boldsymbol{t}}^h$ is replaced by $\bar{\boldsymbol{t}}^h - \bar{\boldsymbol{t}}^h_{mean}$ to satisfy the condition that the traction component associated with constant stress state does not contribute to the rotational forces. It should be noted that the equivalent nodal force vector contains not only the translational forces but also the rotational forces when the traction on an element surface is not constant.

### *3.2. MR-Hx series and associated elements*

Based on the aforementioned concepts, it is possible to establish a series of variable-node hexahedral elements by the selective use of different number of variable nodes. As the first element of the series, the element established in this paper is designated as "MR-H13" which indicate "Mixed formulated element with rotational degrees of freedom – Hexahedral element with 13-nodes". Similarly, MR-H8 is the mixed formulated 8-node hexahedral element with rotational

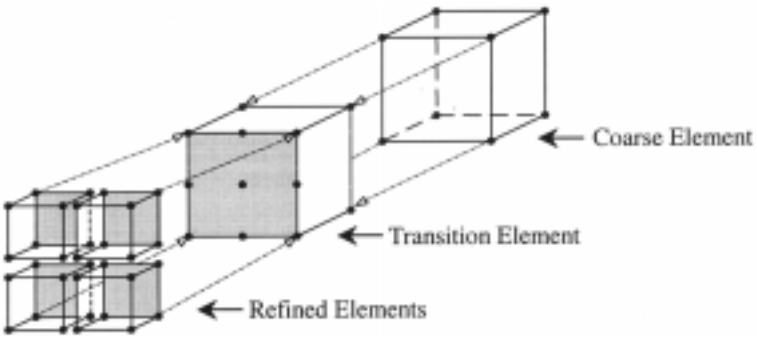


Fig. 5 Use of variable 13-node element as a transition element

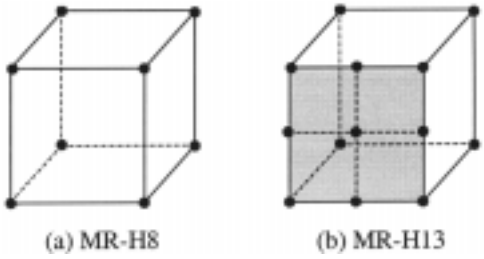


Fig. 6 Element with 1 subdivided face

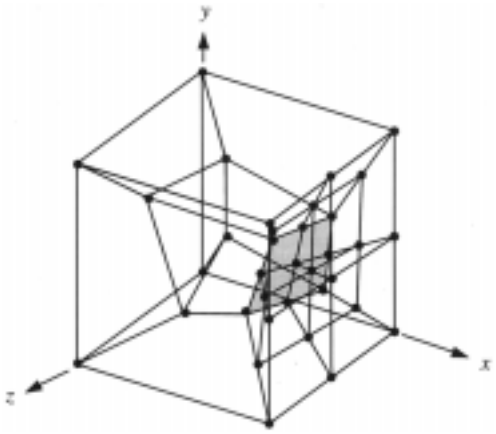


Fig. 7 Patch test model for 3D hexahedral

degrees of freedom. The MR-H13 element is generated by subdividing one of element faces in the mesh refinement process. The face is divided by bisecting in two directions (Fig. 6). The letter "*x*" in MR-H*x* means "variable number of nodes" and designates the elements in the series. Some previously developed variable-node hexahedral elements, such as NC-V1, NC-V2 and C-V2 ( Choi and Lee 1993), are used for the comparison purpose.

## 4. Numerical tests for validation of the element

### *4.1. Basic tests*

To identify the possible spurious mechanisms, which may cause serious drawback of the element, the eigenvalue analyses were carried out for MR-H13 element. For the mixed type formulation, the number of skew symmetric stress parameters is a very important factor for stability of the element. If an adequate number of skew-symmetric stress parameters is used, there are only six zero eigenvalues associated with rigid-body modes for a typical element and no spurious mechanisms are expected to develop. The test results show that the MR-H13 element had only six zero eigenvalues, which exactly represent the six rigid body motion of the element.

In order to check whether the proposed elements are capable of representing constant strain states, the patch tests were carried out. Fig. 7 shows a typical test patch, which contains two types of hexahedral elements, namely, MR-H8 and MR-H13 element. Material properties used for the test are; Young's modulus $E=1.0\times10^6$, and Poisson's ratio $\nu=0.25$. This problem was solved with the

Table 1 Boundary conditions and theoretical results

| Boundary conditions | Theoretical solutions |
|---|---|
| $u=10^{-3}\ (2x+y+z)/2$ | $\varepsilon_x=\varepsilon_y=\varepsilon_z=\gamma_{xy}=\gamma_{yz}=\gamma_{zx}=10^{-3}$ |
| $v=10^{-3}\ (x+2y+z)/2$ | $\sigma_x=\sigma_y=\sigma_z=2000$ |
| $w=10^{-3}\ (x+y+2z)/2$ | $\tau_{xy}=\tau_{yz}=\tau_{zx}=400$ |

prescribed displacement boundary conditions and the obtained results were identical to theoretical solutions (MacNeal and Harder 1985, Table 1).

### *4.2. Cantilever beam under pure bending*

To evaluate the basic performance of the proposed element MR-H13, a cantilever under pure bending about y-axis was tested as shown in Fig. 8(a). For the cantilever beam, the rotational boundary conditions of the fastened end are imposed as symmetric boundary condition on *yz*-plane to model the pure bending state. The material properties are given as $E$=1500, and $\nu$=0.25. The energy equivalent nodal forces of a hexahedral element with rotational degrees of freedom are shown in Fig. 8(b) for the free end of the cantilever beam.

The test meshes composed of three types of hexahedral elements are shown in Fig. 9, i.e., the mesh composed of only MR-H8 elements, a combination of MR-H8 and MR-H13 elements, and the mesh composed of MR-H13 elements only. The vertical displacement and the rotation about y-axis at point A are presented respectively in Table 2 and 3 with the theoretical solution for comparison (Timoshenko and Goodier 1951). Stresses $\sigma_x$ at point B are also listed in Table 4. It is also shown that the proposed MR-13 element, which has rotational degrees of freedom, gives much improved

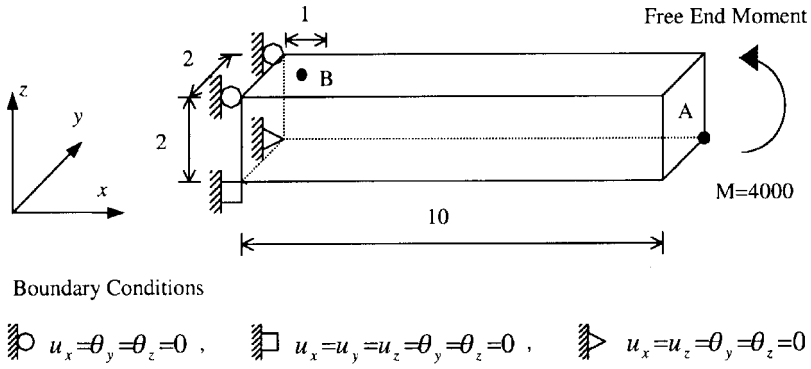


(a) Geometry and boundary conditions

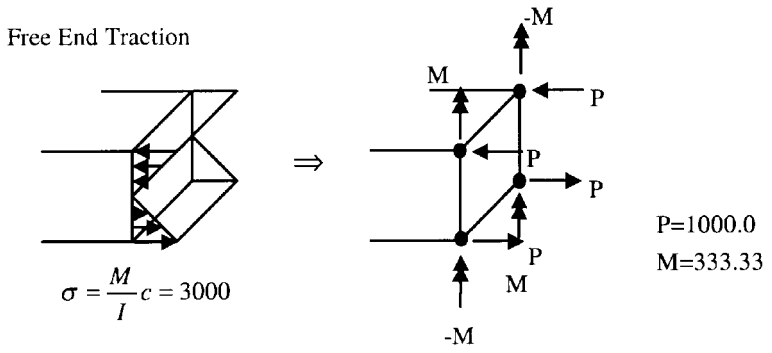


(b) Equivalent nodal forces for bending moment

Fig. 8 Cantilever beam under pure bending

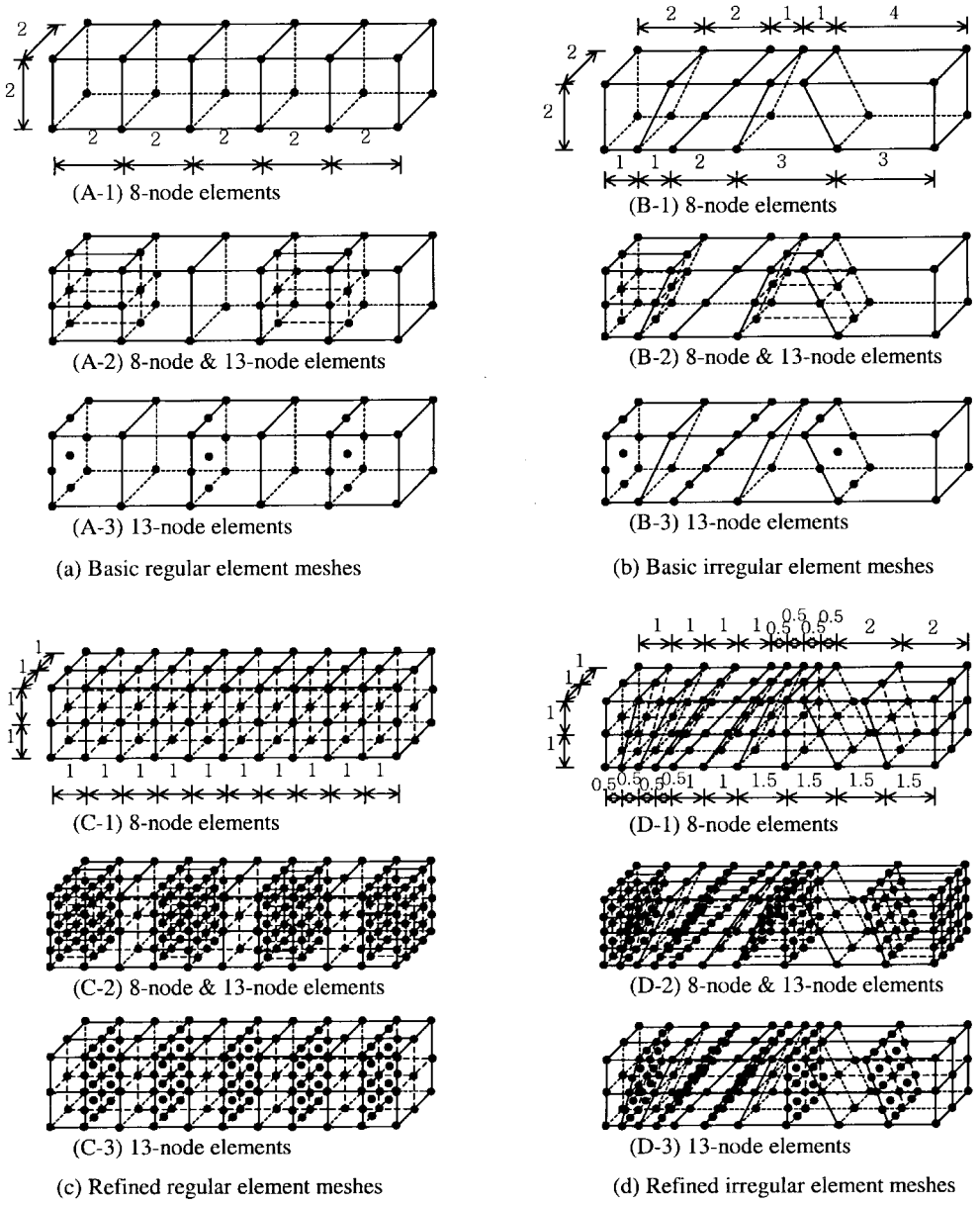


Fig. 9 Several element meshes for numerical test

results over the conventional conforming variable node element (C-V2). When compared with the behaviours of non-conforming variable node elements (NC-V1 and NC-V2), which do not have the roatational degrees of freedom, the MR-H*x* element shows similar or slightly different behavior.

When the distorted meshes are used the accuracy of solution obtained by MR-H13 is generally superior over the accuracies obtained by C-V2, NC-V1, and NC-V2.

Table 2 Vertical displacement of cantilever beam under pure bending (point A)

| Mesh / Type | Basic regular element meshes | | | Basic irregular element meshes | | |
|---|---|---|---|---|---|---|
| | 8-node (A-1) | 8&13-node (A-2) | 13-node (A-3) | 8-node (B-1) | 8&13-node (B-2) | 13-node (B-3) |
| C-V2 | 66.67 | 69.62 | 69.18 | 44.38 | 47.37 | 49.27 |
| NC-V1 | 100.00 | 101.04 | 99.91 | 87.45 | 80.13 | 91.13 |
| NC-V2 | 100.00 | 99.96 | 99.92 | 87.45 | 79.55 | 90.82 |
| MR-H*x* | 93.75 | 100.46 | 96.96 | 81.09 | 86.32 | 90.79 |
| Mesh / Type | Refined regular element meshes | | | Refined irregular element meshes | | |
| | 8-node (C-1) | 8&13-node (C-2) | 13-node (C-3) | 8-node (D-1) | 8&13-node (D-2) | 13-node (D-3) |
| MR-H*x* | 98.21 | 100.03 | 99.18 | 96.33 | 99.24 | 97.03 |
| Theory | 100.00 | | | | | |

Table 3 Rotation of cantilever beam under pure bending (point A)

| Mesh / Type | Basic regular element meshes | | | Basic irregular element meshes | | |
|---|---|---|---|---|---|---|
| | 8-node (A-1) | 8&13-node (A-2) | 13-node (A-3) | 8-node (B-1) | 8&13-node (B-2) | 13-node (B-3) |
| MR-H*x* | −18.75 | −19.95 | −19.50 | −16.77 | −17.24 | −17.89 |
| Mesh / Type | Refined regular element meshes | | | Refined irregular element meshes | | |
| | 8-node (C-1) | 8&13-node (C-2) | 13-node (C-3) | 8-node (D-1) | 8&13-node (D-2) | 13-node (D-3) |
| MR-H*x* | −19.64 | −19.99 | −19.89 | −19.25 | −19.91 | −19.59 |
| Theory | −20.00 | | | | | |

Table 4 Stresses of cantilever beam under pure bending (point B)

| Mesh / Type | Basic regular element meshes | | | Basic irregular element meshes | | |
|---|---|---|---|---|---|---|
| | 8-node (A-1) | 8&13-node (A-2) | 13-node (A-3) | 8-node (B-1) | 8&13-node (B-2) | 13-node (B-3) |
| C-V2 | −2200 | −2208 | −2208 | −1736 | −2049 | −1738 |
| NC-V1 | −3000 | −3175 | −3000 | −2262 | −2953 | −2402 |
| NC-V2 | −3000 | −2992 | −2999 | −2262 | −2802 | −2396 |
| MR-H*x* | −3000 | −3070 | −3024 | −2405 | −3369 | −2484 |
| Mesh / Type | Refined regular element meshes | | | Refined irregular element meshes | | |
| | 8-node (C-1) | 8&13-node (C-2) | 13-node (C-3) | 8-node (D-1) | 8&13-node (D-2) | 13-node (D-3) |
| MR-H*x* | 3071 | 3005 | 2977 | 3001 | 2979 | 2889 |
| Theory | −3000 | | | | | |

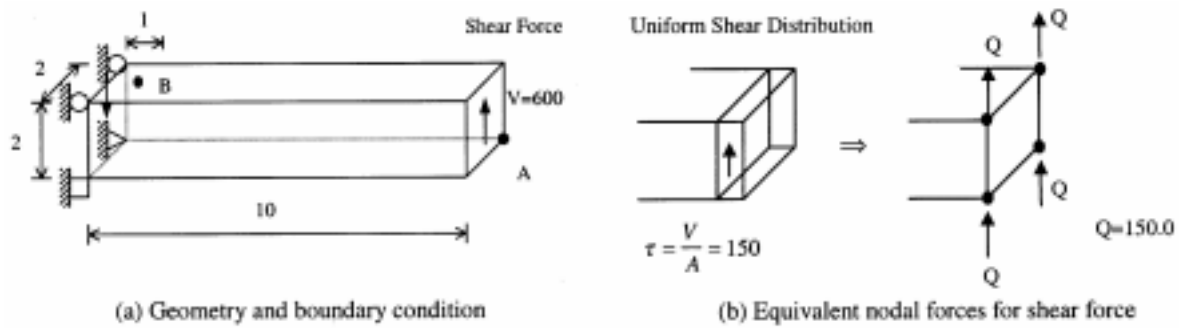


Fig. 10 Cantilever beams under tip shear forces

### 4.3. Cantilever beam under shear load

The same cantilever beam of the previous example was tested under a shear force (See Fig. 10). The test meshes which are composed of 8-node and 13-node hexahedral elements are the same as shown in Fig. 9 and the same material properties as the previous example ($E$=1500, $\nu$=0.25) are used. It is assumed that the shear force is acting on the free end of cantilever beam with the uniform distribution for simplicity.

The rotations about $y$-axis at point $A$ under shear load are shown in Table 5 and 6 along with the theoretical solutions for comparison. In Table 6, no comparisons are made since the elements C-V2, NC-V1, and NC-V2 do not have rotational degrees of freedom. The stress $\sigma_x$ at point B is also shown in Table 7. Similar trends of solutions as the previous example are obtained.

### 4.4. Convergence of MR-Hx elements

Test results listed in Tables 2 to 7 show respectively the numerical test results for basic element

Table 5 Vertical displacement of cantilever beam under shear force (point A)

| Mesh / Type | Basic regular element meshes | | | Basic irregular element meshes | | |
|---|---|---|---|---|---|---|
| | 8-node (A-1) | 8&13-node (A-2) | 13-node (A-3) | 8-node (B-1) | 8&13-node (B-2) | 13-node (B-3) |
| C-V2 | 68.45 | 71.41 | 70.87 | 49.33 | 52.94 | 54.25 |
| NC-V1 | 101.40 | 102.30 | 101.35 | 89.89 | 82.85 | 93.22 |
| NC-V2 | 101.40 | 101.31 | 100.28 | 89.89 | 82.13 | 92.82 |
| MR-H$x$ | 96.73 | 102.24 | 99.88 | 84.02 | 89.25 | 93.48 |
| Mesh / Type | Refined regular element meshes | | | Refined irregular element meshes | | |
| | 8-node (C-1) | 8&13-node (C-2) | 13-node (C-3) | 8-node (D-1) | 8&13-node (D-2) | 13-node (D-3) |
| MR-H$x$ | 100.39 | 102.47 | 101.68 | 98.27 | 101.56 | 99.17 |
| Theory | 102.625 | | | | | |

Table 6 Rotation of cantilever beam under shear force (point A)

| Mesh / Type | Basic regular element meshes | | | Basic irregular element meshes | | |
|---|---|---|---|---|---|---|
| | 8-node (A-1) | 8&13-node (A-2) | 13-node (A-3) | 8-node (B-1) | 8&13-node (B-2) | 13-node (B-3) |
| MR-H*x* | −14.30 | −15.29 | −15.00 | −12.45 | −13.05 | −13.72 |
| Mesh / Type | Basic regular element meshes | | | Basic irregular element meshes | | |
| | 8-node (C-1) | 8&13-node (C-2) | 13-node (C-3) | 8-node (D-1) | 8&13-node (D-2) | 13-node (D-3) |
| MR-H*x* | −14.83 | −15.24 | −14.96 | −14.41 | −15.04 | −14.51 |
| Theory | −15.02 | | | | | |

Table 7 Stresses of cantilever beam under shear force (point B)

| Mesh / Type | Basic regular element meshes | | | Basic irregular element meshes | | |
|---|---|---|---|---|---|---|
| | 8-node (A-1) | 8&13-node (A-2) | 13-node (A-3) | 8-node (B-1) | 8&13-node (B-2) | 13-node (B-3) |
| C-V2 | −2972 | −2991 | −2983 | −2415 | −2836 | −2403 |
| NC-V1 | −4050 | −4269 | −4059 | −3097 | −4039 | −3278 |
| NC-V2 | −4050 | −4051 | −4048 | −3097 | −3853 | −3254 |
| MR-H*x* | −4092 | −4176 | −4129 | −3445 | −4489 | −3526 |
| Mesh / Type | Refined regular element meshes | | | Refined irregular element meshes | | |
| | 8-node (C-1) | 8&13-node (C-2) | 13-node (C-3) | 8-node (D-1) | 8&13-node (D-2) | 13-node (D-3) |
| MR-H*x* | −4146 | −4071 | −4019 | −4104 | −4091 | −3958 |
| Theory | −4050 | | | | | |

meshes and refined element meshes. In this test, the both cases of regular and distorted element shape are considered. The test results with refined meshes indicate the good convergence characteristics of MR-H*x* elements.

### *4.5. Application to an engineering problem*

To show the applicability of the presented MR-H13 element in local mesh refiement, the upper part of a movable shoe is considered (Fig. 11). For simplicity only 1/4 part of the shoe is actually modeled by MR-H8 and MR-H13 elements, and the boundary condition for lower surface is given as a roller support, i.e., displacements are restricted only in the radial direction. MR-H13 elements were effectively used in the mesh generation in the transition zone (Fig. 12). A uniform pressure of total 6000 tf is acting on the top surface of the model. Material properties are given as Young's modulus $E=2.1\times10^4$ kgf/mm$^2$, Poisson's ratio $\nu=0.3$. Analysis result shows the vertical displacement as 0.11230 mm at a center point of top suface (Fig. 13), and the effective stress distribution on the surface of mesh are shown in Fig. 14.

This practical example shows that as the mesh gradation by using variable-node elements can

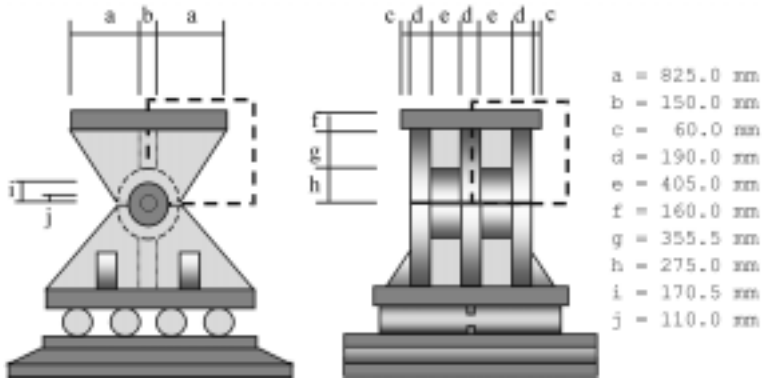


Fig. 11 Movable shoe

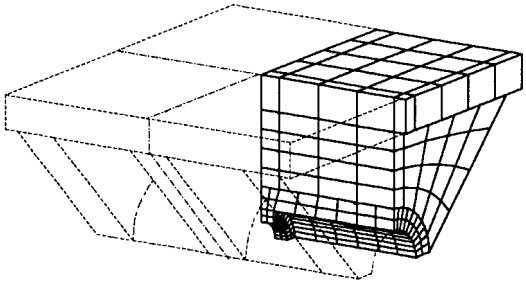

Fig. 12 1/4 model of upper shoe part by MR-H8 and MR-H13

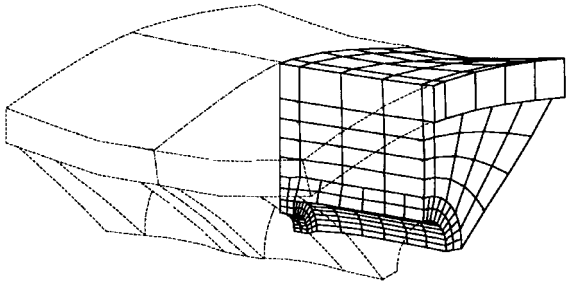

Fig. 13 Deformed mesh under constant pressure on top surface

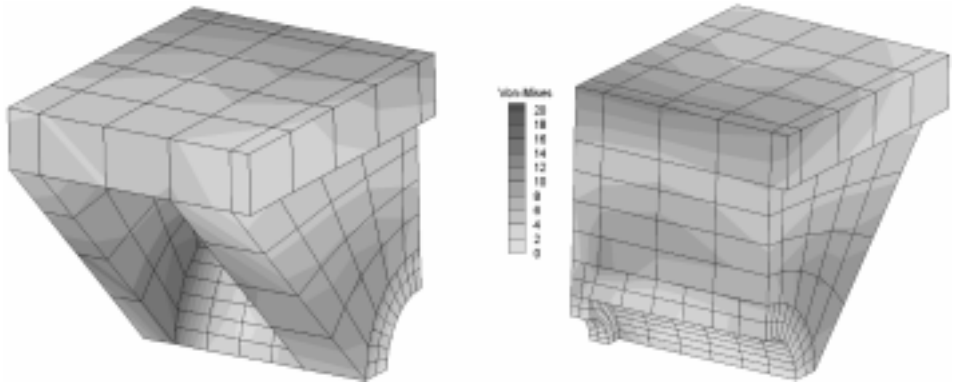

Fig. 14 Effective stress contour on element faces (tf/mm$^2$)

maintain the mesh regularity in refinement process, the variable node element is very useful for adaptive mesh refinement where the finer mesh is connected to the coarser mesh.

## 7. Conclusions

In this paper, the 13-node hexahedral element with rotational degrees of freedom which is

designated as MR-H13 has been presented. A mixed formulation, which employs skew-symmetric stress and rotation field, is used in the formulation of the presented element. The element is formed by adding five additional nodes to an 8-node MR-H8 element, i.e., four mid-edge nodes and one node at the center of an element face. These additional nodes enable the element to be effectively connected to four subdivided elements to form the transitional zone where the coarse mesh is connected to a finer one.

From the numerical tests, it has been verified that the proposed element pass the patch tests and produce no spurious zero energy mechanisms. The test results also show the good convergence of the element. The improvement of the element behavior achieved by employing the independent rotation fields over the original element was significant and comparable to the improvement achieved by addition of non-conforming displacement modes without addition of rotational degrees of freedom (NC-V1 and NC-V2 elements). It is expected that even further improvement can be achieved by addition of the selected serveral non-conforming modes in the present element. The MR-H13 elements can provide an excellent scheme to modeling and analyzing the complex structures, where the local refinement is required. Also MR-H13's six degrees of freedom per node will allow easy connection to other types of finite elements which have six degrees of freedom per node.

It is expected in the future that based on this initial study a series of variable node hexahedral element can be developed by the selection of the number and locations of variable nodes.

## References

Allman, D.J. (1984), "A compatible triangular element including vertex rotations for plane elasticity analysis", *Computers and Structures*, **19**(2), 1-9.

Chang, K.H. and Choi, K.K. (1992), "An error analysis and mesh adaptation method for shape design of structural components", *Comp. and Struct.*, **44**(6), 1275-1289.

Choi, C.K. and Park, Y.M. (1989), "Nonconforming transition plate bending elements with variable mid-side nodes", *Comp. and Struct*., **32**(2), 295-304.

Choi, C.K. and Lee, N.H. (1993), "Three dimensional solid elements for adaptive mesh gradation", *Structural Engineering and Mechanics*, **1**, 61-74.

Choi, C.K. and Lee, W.H. (1995), "Transition membrane elements with drilling freedom for local mesh refinements", *Structural Engineering and Mechanics*, **3**(1), 75-89.

Choi, C.K. and Chung, K.Y. (1995), "Three-dimensional variable node solid element with drilling degrees of freedom", *Proceedings of 6th International Conference on Computing in Civil and Building Eng.*, Berlin, Germany, July, 521-528.

Choi, C.K., Chung, K.Y. and Lee, N.H. (1996), "Three-dimensional non-conforming 8-node solid elements with rotational degrees of freedom", *Structural Engineering and Mechanics*, **4**(5), 569-586.

Cook, R.D. (1981), *Concept and Application of Finite Element Analysis*, 2nd Ed., John Wiley & Sons, New York.

Delvoo, P.R. (1991), "Three-dimensional adaptive finite element strategy", *Comp. and Struct*., **38**(2), 121-130.

Gargo, J.P. *et al*. (1983), "A posteriori error analysis and adaptive process in the finite element method: Part 2 - Adaptive mesh refinement", *Int., J. for Numer. Methods in Eng*., **19**, 1621-1656.

Gupta, A.K. (1978), "A finite element for transition from a fine to a coarse grid", *Int. Journal for Numer. Meth. in Eng*., **12**(1), 35-45.

Hughes, T.J.R. and Brezzi, F. (1989), "On drilling degrees of freedom", *Comp. Methods Appl. Mech. Eng*., **72**, 105-121.

Ibrahimbegovic, A. and Wilson, E.L. (1991), "Thick shell and solid finite elements with independent rotation

fields", *Int. J. Numer. Methods Eng*., **31**, 1393-1414.
Iron, B.M. (1971), "Quadrature rules for brick-based finite elements", *Int. Journal for Numerical Methods in Engineering*, **3**, 293-294.
MacNeal, R.H. and Harder, R.L. (1985), "A proposed standard set of problems to test finite element accuracy", *Finite Elements in Analysis and Design*, **1**, 3-20.
Reissner, E. (1965), "A note on variational theorems in elasticity", *Int. J. Solids and Structures*, **1**, 93-95.
Timoshenko, S. and Goodier, J.N. (1951), *Theory of Elasticity*, McGraw-Hill, New York.
Yunus, S.M., Pawlak, T.P. and Cook, R.D. (1991), "Solid elements with rotational degrees of freedom: part 1-hexahedron elements", *Int. J. Numer. Methods Eng*., **31**, 573-592.